CHAPTER SEVEN

Characterization of the [NiFeSe] hydrogenase from *Desulfovibrio vulgaris* Hildenborough

Sónia Zacarias[a], Marisela Vélez[b], Marcos Pita[b], Antonio L. De Lacey[b,*], Pedro M. Matias[a,c,*], Inês A.C. Pereira[a,*]

[a]Instituto de Tecnologia Química e Biológica António Xavier, Universidade Nova de Lisboa, Oeiras, Portugal
[b]Instituto de Catálisis y Petroleoquímica, CSIC, Madrid, Spain
[c]iBET, Instituto de Biologia Experimental e Tecnológica, Oeiras, Portugal
*Corresponding authors: e-mail address: alopez@icp.csic.es; matias@itqb.unl.pt; ipereira@itqb.unl.pt

Contents

Methods in Enzymology, Volume 613
ISSN 0076-6879
https://doi.org/10.1016/bs.mie.2018.10.003

Abstract

The [NiFeSe] hydrogenases are a subgroup of the well-characterized family of [NiFe] hydrogenases, in which a selenocysteine is a ligand to the nickel atom in the binuclear NiFe active site instead of cysteine. These enzymes display very interesting catalytic properties for biological hydrogen production and bioelectrochemical applications: high H_2 production activity, bias for H_2 evolution, low H_2 inhibition, and some degree of O_2 tolerance.

Here we describe the methodologies employed to study the [NiFeSe] hydrogenase isolated from the sulfate-reducing bacteria *D. vulgaris* Hildenborough and the creation of a homologous expression system for production of variant forms of the enzyme.

1. Introduction

[NiFe] hydrogenases are the most abundant and well-characterized group of hydrogenases. Their active site contains a NiFe binuclear center bound to the protein chain by four cysteine residues, two of which bridge the two metals while the other two are bound terminally to the Ni. The [NiFeSe] hydrogenases are a subclass of the [NiFe] hydrogenases in which a selenocysteine (Sec) replaces cysteine as one of the nickel ligands. Sec is codified by the same codon as "stop" (UGA), and a dedicated cellular machinery is needed to recode this codon as "selenocysteine" instead of "stop" and to insert Sec correctly into the protein: this means that the use of Sec instead of Cys is obviously very costly to the cell (Papp, Lu, Holmgren, & Khanna, 2007). The evolutionary advantage of using Sec over Cys is associated not only with a higher catalytic efficiency but most importantly with the ability of Sec to react with O_2 in a readily reversible manner and thus resist oxidative inactivation (Maroney & Hondal, 2018; Reich & Hondal, 2016). This concept was recently confirmed also for the *D. vulgaris* Hildenborough [NiFeSe] hydrogenase, through production of a variant where the Sec residue was replaced by a Cys. This variant exhibited reduced catalytic activity and a higher sensitivity to O_2 inactivation, confirming the role of selenium in protecting against oxidative damage (Marques et al., 2017). The Sec/Cys hydrogenase variant also displayed a much reduced Ni incorporation, suggesting the direct involvement of Sec in the maturation of the active site.

[NiFeSe] hydrogenases present interesting catalytic properties in comparison with other hydrogenases: (i) high catalytic activities and a bias for H_2 evolution (Baltazar et al., 2011); (ii) lower inhibition by H_2

(Parkin, Goldet, Cavazza, Fontecilla-Camps, & Armstrong, 2008); (iii) some degree of tolerance to O_2, as they do not form inactive Ni(III) states (Teixeira et al., 1987), and can be rapidly reactivated under reducing conditions (Parkin et al., 2008). These properties have been exploited in biocatalytic applications of [NiFeSe] hydrogenases for photo- and electrochemical H_2 production (Caputo et al., 2014; Caputo, Wang, Beranek, & Reisner, 2015; Dong et al., 2018; Lee, Park, Fontecilla-Camps, & Reisner, 2016; Mersch et al., 2015; Reisner, Fontecilla-camps, & Armstrong, 2009; Reisner, Powell, Cavazza, Fontecilla-Camps, & Armstrong, 2009; Rüdiger et al., 2010; Sakai, Mersch, & Reisner, 2013; Tapia et al., 2016) and also for electrochemical ATP synthesis (Gutiérrez-Sanz et al., 2016).

To date [NiFeSe] hydrogenases have been reported only in sulfate-reducing bacteria and methanogenic archaea (Baltazar et al., 2011). From these groups only a few [NiFeSe] hydrogenases have been isolated, namely, those from the sulfate-reducing bacteria *Desulfovibrio salexigens* (Teixeira et al., 1986), *Dm. baculatum* (Teixeira et al., 1987), *D. vulgaris* Hildenborough (Valente et al., 2005), and *D. vulgaris* Miyazaki (Nonaka, Nguyen, Yoon, & Ogo, 2013), and from the methanogens *Methanococcus vannielii* (Yamazaki, 1982) and *Methanococcus voltae* (Muth, Morschel, & Klein, 1987).

In this chapter, we describe the methods employed to express, purify, and characterize forms of the [NiFeSe] hydrogenase from *D. vulgaris* Hildenborough, which is an anaerobic sulfate-reducing organism that can use H_2 as energy source or produce H_2 fermentatively or during syntrophic growth. The *D. vulgaris* Hildenborough genome encodes seven hydrogenases of the [FeFe] and [NiFe] families (Pereira et al., 2011). Four of these are periplasmic: the [FeFe] hydrogenase (Hyd), two [NiFe] hydrogenases (HynAB-1 and HynAB-2), and a [NiFeSe] hydrogenase (HysAB), whereas three lie within or face cytoplasm, namely, the two membrane-associated energy-conserving hydrogenases, Ech and Coo, and a soluble [FeFe] hydrogenase (Pereira et al., 2011).

The *D. vulgaris* Hildenborough [NiFeSe] hydrogenase (HysAB) is a membrane-associated periplasmic-facing protein, consisting of two subunits, a large subunit (HysA) with molecular mass 63 kDa and a small subunit (HysB) with molecular mass 35 kDa (Valente et al., 2005). The membrane association is achieved through a lipidic group linked to Cys4 at the N-terminus of the large subunit. HysA was the first example reported of a bacterial lipoprotein where the signal peptide is limited to a conserved four-residue lipobox (Fig. 1), since the other regions present in typical

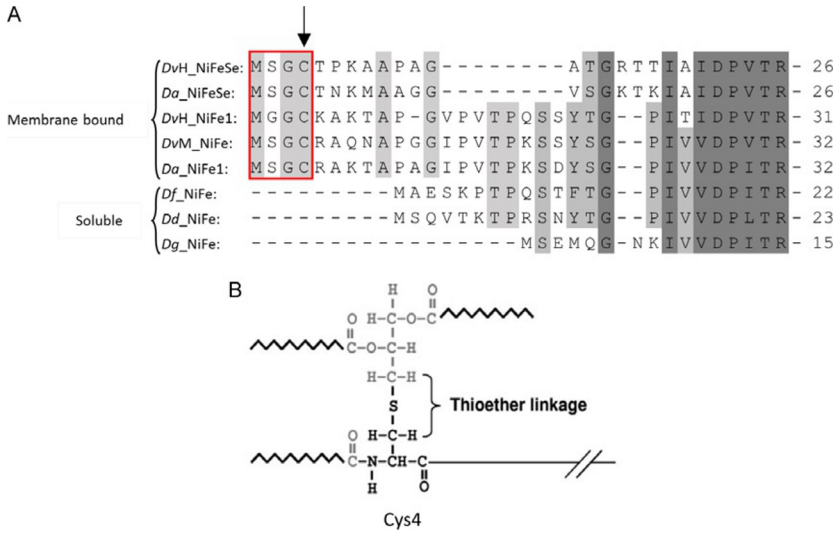

Fig. 1 (A) Sequence alignment of the large subunit N-terminus of several *Desulfovibrionaceae* hydrogenases. The conserved four-residue lipobox is highlighted by the *red box*, and the cysteine, where the lipid group will bind, by an *arrow*. Membrane-associated hydrogenases: *D. vulgaris* Hildenborough [NiFeSe] (*Dv*H_NiFeSe); *D. alaskensis* [NiFeSe] (*Da*_NiFeSe); *D. vulgaris* Hildenborough [NiFe]1 (*Dv*H_NiFe1); *D. vulgaris* Miyazaki [NiFe] (*Dv*M_NiFe); *D. alaskensis* [NiFe]1 (*Da*_NiFe1). Soluble hydrogenases: *D. fructosovorans* [NiFe] (*Df*_NiFe); *D. desulfuricans* ATTC 27774 [NiFe] (*Db*_NiFe); *D. gigas* [NiFe] (*Dg*_NiFe). (B) Representation of the *N*-acyl-*S*-diacylglyceryl group bound to Cys4.

lipoprotein signal peptides, involved in recognition and transport by the general secretory pathway (Sec pathway), are absent (Valente et al., 2007). The reason behind this difference is that HysA is translocated by the Tat pathway in complex with HysB (Rodrigue et al., 1999; Valente et al., 2007), which contains a standard Tat signal peptide. Thus, HysA was the first example of a bacterial lipoprotein translocated through the Tat and not the Sec pathway (Valente et al., 2007).

The main physiological role of HysAB is in H_2 oxidation, with the periplasmic type-I cytochrome c_3 (TpIc_3) as the physiological electron acceptor (Pereira, Romão, Xavier, Le Gall, & Teixeira, 1998; Valente et al., 2005). In solution assays this enzyme is biased toward H_2 production, presenting very high activities: 4787 U mg^{-1} (7008 s^{-1}) and 6908 U mg^{-1} (10,132 s^{-1}) (Table 1), in the presence of detergent or phospholipids, respectively.

Table 1 Catalytic activities for *D. vulgaris* Hildenborough [NiFeSe] hydrogenase

	$[NiFeSe]_m$ hydrogenase	**$[NiFeSe]_s$ hydrogenase**	**$[NiFeSe]_r$ hydrogenase**
H_2 evolution	$4787\,U\,mg^{-1}$ $(7008\,s^{-1})^a$ $6908\,U\,mg^{-1}$ $(10{,}132\,s^{-1})^b$	$860\,U\,mg^{-1}$ $(1261\,s^{-1})$	$5640\,U\,mg^{-1}$ $(8272\,s^{-1})$
H_2 uptake	$900\,U\,mg^{-1}$ $(1320\,s^{-1})$	N.D.	$3037\,U\,mg^{-1}$ $(4454\,s^{-1})$
H_2 photoproduction	N.D.	N.D.	$672\,U\,mg^{-1}$ $(986\,s^{-1})$
Isotopic D_2–H^+ exchange activity			
$HD + H_2$ evolution	$140\,U\,mg^{-1}$ $(205\,s^{-1})$	N.D.	$1300\,U\,mg^{-1}$ $(2000\,s^{-1})$

H_2 evolution and uptake activities for $[NiFeSe]_m$ hydrogenase in the presence of detergent[a] and phospholipids[b] (Marques, Coelho, Pereira, & Matias, 2013; Valente et al., 2005). H_2 evolution activity for $[NiFeSe]_s$ hydrogenase (Valente et al., 2005). H_2 evolution activity for $[NiFeSe]_r$ hydrogenase (Marques et al., 2017) and H_2-photoproduction activity (Tapia et al., 2016). Isotopic exchange activities for $[NiFeSe]_m$ hydrogenase in the presence of detergent (Gutiérrez-Sanz et al., 2013) and $[NiFeSe]_r$ hydrogenase (Marques et al., 2017). N.D., not determined.

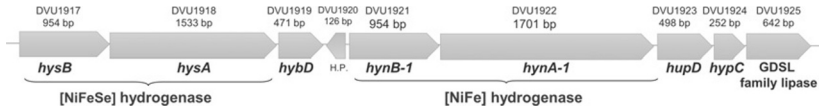

Fig. 2 The *D. vulgaris* Hildenborough gene locus containing the [NiFeSe] hydrogenase genes is approximately 8 kb long. It comprises the genes for the small and large subunits of [NiFeSe] hydrogenase (*hysB* and *hysA*) and [NiFe]1 hydrogenase (*hynB* and *hynA*), a set of maturation genes (*hybD*, *hupD*, *hypC*), a hypothetical protein (H.P.), and a gene coding for an GPLS family lipase.

Besides the membrane-associated form of the [NiFeSe] hydrogenase (herein named $[NiFeSe]_m$ hydrogenase), a soluble form ($[NiFeSe]_s$ hydrogenase) also exists in the cell, which lacks the first 11 residues of the large subunit and the hydrophobic group. This soluble form may be produced by cleavage of the lipidic group in $[NiFeSe]_m$ hydrogenase by a lipase encoded in the same locus (Fig. 2) as the [NiFeSe] hydrogenase genes (Valente et al., 2007), or by autoproteolytic degradation, since its presence increases in aged preparations of the $[NiFeSe]_m$ hydrogenase (Valente et al., 2005). The reported catalytic activities for native $[NiFeSe]_s$ hydrogenase ($860\,U\,mg^{-1}$ for H_2 production) (Marques et al., 2013; Valente et al., 2005) were always much lower than those of $[NiFeSe]_m$ hydrogenase.

Recently, a recombinant version of the soluble [NiFeSe] hydrogenase ([NiFeSe]$_r$ hydrogenase) was created (Marques et al., 2017). It contains a strep-tag in the N-terminus of the large subunit to facilitate purification and is homologously expressed in *D. vulgaris* Hildenborough, given the known specificity of the maturation proteins and selenocysteine insertion machinery. The [NiFeSe]$_r$ hydrogenase displays a high H_2-production activity of $5640 \pm 260\,U\,mg^{-1}$ ($8272 \pm 381\,s^{-1}$) (Table 1) which is comparable with the activities reported for the native membrane form (Valente et al., 2005). This result suggests that the low activities obtained for the native soluble form of the enzyme were mainly caused by the long purification protocol, rather than by the loss of the lipidic N-terminal tail of enzyme.

The structure of *D. vulgaris* Hildenborough [NiFeSe] hydrogenase was solved in 2010 (Fig. 3A) (Marques, Coelho, De Lacey, Pereira, & Matias, 2010) and, as observed for the *D. baculatum* enzyme (Garcin et al., 1999), revealed an overall arrangement very similar to the standard [NiFe] hydrogenases, with major differences restricted to the active site and the presence of a medial [4Fe4S] cluster in the small subunit, rather than a [3Fe4S] cluster. The structure of the *D. vulgaris* Hildenborough [NiFeSe] hydrogenase was the first structure reported for an oxidized hydrogenase of the [NiFe] family that did not contain an oxide species bridging the metals in the active site (Marques et al., 2010). However, evidence of O_2 damage was present in the terminal Cys75 ligand of Ni, which was oxidized to a sulfenate/sulfinate. Also, the proximal FeS cluster was partially oxidized to $Fe_4S_3O_2$ (Fig. 3B), but this oxidative modification was reversed upon reduction (Marques et al., 2010, 2013); it has also been observed in the structure of [NiFe] hydrogenase of *D. desulfuricans* ATCC (Matias et al., 2001). The active site of the oxidized *D. vulgaris* Hildenborough [NiFeSe] hydrogenase is found in three different conformations (Fig. 3C). In two of them the Se atom is bound to an exogenous sulfur atom (conformers I and II), while the third has a direct Ni–Se bond (conformer III) and corresponds to the conformation of the reduced enzyme. The extra sulfur atom in conformers I and II induces a Sec conformation that shields the NiFe site from contact with oxygen, preventing inactivation associated with bridging oxide ligands (Marques et al., 2013, 2017).

Recently, it was proposed that the sulfur atom at the active site results from the sulfide produced from the bacterial metabolism, which may be involved in repair of oxidative damage at the active site (Maroney & Hondal, 2018). This is supported by the fact that in the reduced form of the enzyme the sulfide group can occupy a cavity in the enzyme (Garcin et al., 1999; Marques et al., 2017).

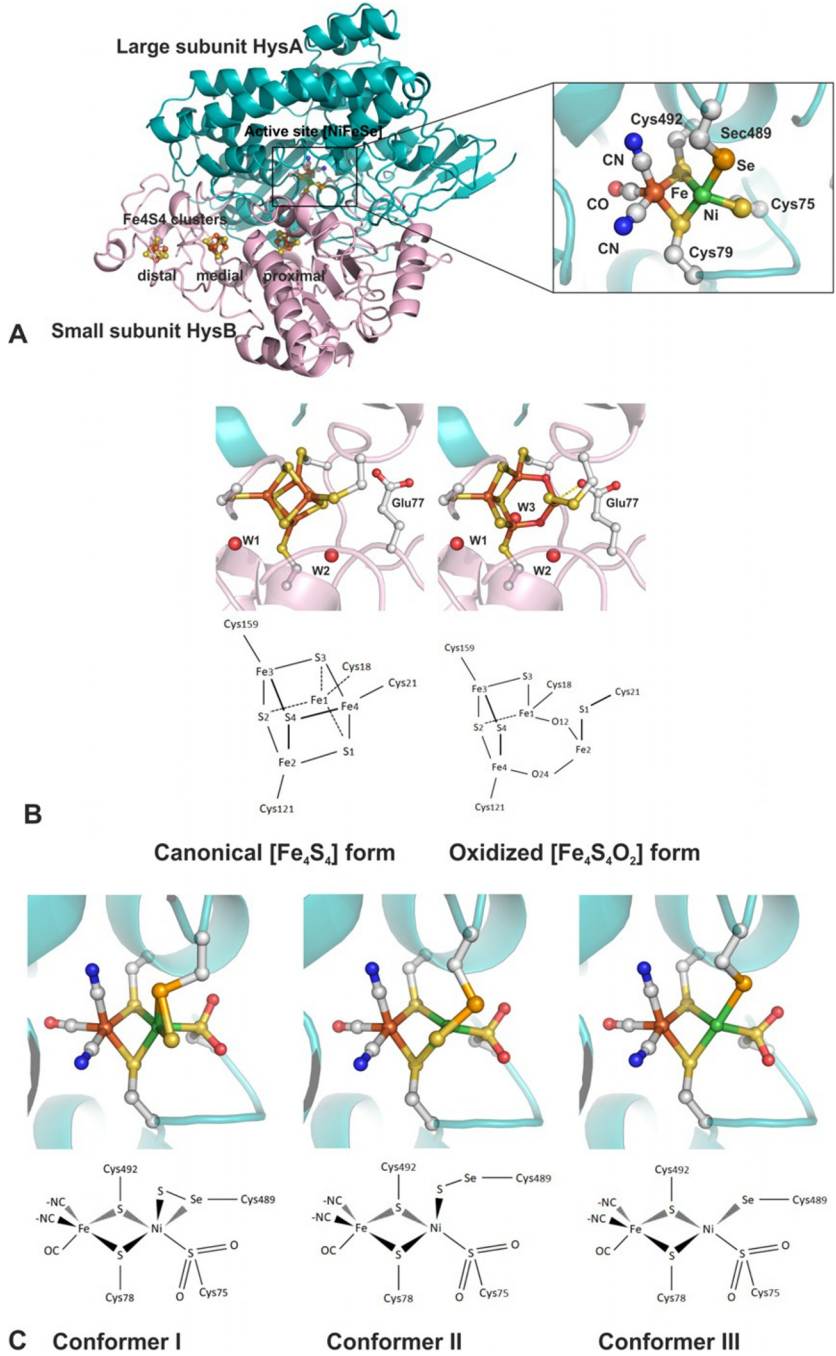

Fig. 3 See legend on next page.

2. Preparation of the native [NiFeSe] hydrogenase from *D. vulgaris* Hildenborough

2.1 Growth of *D. vulgaris* Hildenborough for expression of the [NiFeSe] hydrogenase

The strain used is *D. vulgaris* Hildenborough (DSM 644). In this organism the expression of the periplasmic hydrogenases is regulated by the growth substrate, H_2 concentration, and by Ni and Se levels (Caffrey et al., 2007; Valente, Almeida, Pacheco, Saraiva, & Pereira, 2006). Although a higher protein yield can be obtained from cells grown with H_2, the *D. vulgaris* Hildenborough is routinely purified from cells grown in standard lactate–sulfate conditions. To induce the expression of the [NiFeSe] hydrogenase and downregulate the expression of the Hyd and HynAB-1/2 enzymes, selenium must be present in the medium. In this case the [NiFeSe] hydrogenase becomes the dominant hydrogenase, irrespective of the electron donor used (Valente et al., 2006).

Fig. 3 (A) The 3D structure of the *D. vulgaris* Hildenborough [NiFeSe] hydrogenase (taken from PDB 5JSK). *Left*: overall view. The two protein chains are displayed as cartoons; the [NiFeSe] active site, its coordinating ligands, and the three [4Fe4S] clusters are shown in ball-and-stick representation. *Right:* Close-up view of the active site. The [NiFe] binuclear center and the side chains of the coordinating protein ligands are shown in ball-and-stick representation. Atom colors are *brown* for iron, *green* for nickel, *gold* for sulfur, *red* for oxygen, *light gray* for carbon, *blue* for nitrogen, and *orange* for selenium. The HysA protein chain is represented as a semitransparent cartoon. (B) The canonical and the oxidized forms of the proximal [4Fe4S] cluster in the structure of *D. vulgaris* [NiFeSe] hydrogenase. The proximal cluster becomes partially oxidized under aerobic crystallization conditions. This oxidized form is not observed after reducing with H_2/dithionite or anaerobic crystallization. In the oxidized form, Glu77 approaches atom Fe2 within coordinating bond distance. The three water molecules represented surround the proximal cluster and are conserved in all known structures of [NiFe] and [NiFeSe] hydrogenases with a [4Fe4S] proximal cluster coordinated by four cysteine residues. (C) The three Sec conformers in the active site of *D. vulgaris* [NiFeSe] hydrogenase. *Conformer I* (taken from PDB 3ZE6) contains an exogenous sulfur atom (presumably as HS^-) bound to both the Ni and Se atoms, and is predominant in crystals obtained aerobically; *Conformer II* (taken from PDB 3ZE8) also contains an exogenous sulfur atom (presumably as HS^-) bound to both the Ni and Se atoms, and is predominant in crystals reoxidized under air after reduction with H_2/dithionite or anaerobic crystallization; *Conformer III* (taken from PDB 3ZE7) represents the active form of the enzyme and is predominant after crystal reduction with H_2/dithionite or anaerobic crystallization. The three crystal structures were obtained from an aerobically purified enzyme sample, hence the oxidative damage at Cys75.

The medium used is the modified Postgate C medium (Postgate, 1984), with the following composition: 40 m*M* sodium lactate, 18 m*M* Na_2SO_4, 18.5 m*M* NH_4Cl, 1 g/L yeast extract, 3.7 m*M* KH_2PO_4, 1 m*M* sodium citrate tribasic dihydrate, 0.9 m*M* sodium thioglycolate, 0.6 m*M* ascorbic acid, 0.4 m*M* $CaCl_2{\cdot}2H_2O$, 0.2 m*M* $MgSO_4{\cdot}7H_2O$, 26 μ*M* $FeSO_4{\cdot}7H_2O$, 1 μ*M* $NiCl_2{\cdot}6H_2O$, 1 μ*M* $NaSeO_3{\cdot}5H_2O$, and 0.001% (w/v) resazurin (giving a pink color when oxygen is present). The pH is adjusted to 7.2 ± 0.1 with HCl. Cells are grown at 37°C, always in anaerobic conditions, achieved by degassing the medium solution and replacing the atmosphere with N_2.

To grow *D. vulgaris* Hildenborough, 1 mL of a cell suspension freezer stock (stored in vials at −80°C in 10% (v/v) glycerol) is added to 10 mL medium and grown overnight. A 10% (v/v) inoculum is used for all growth transfers. Depending on the amount of protein required, the growth volume can vary from 30 to 300 L. The 30 L growth volume is performed using three 10 L size Schott flasks with a small headspace filled with N_2. The 300 L growth is performed in a bioreactor with N_2 in the headspace.

The initial downstream processes are usually performed under air, with no major impact on the [NiFeSe] hydrogenase activity, given the presence of reducing sulfide in the crude cell extract. Cells are transferred to centrifuge bottles inside the fume hood to avoid inhalation of hydrogen sulfide and collected by centrifuging them at 11,000 *g*, 4°C. Cells can be stored at −80°C for several years without affecting the enzyme activity.

2.2 Purification of the membrane form of the [NiFeSe] hydrogenase

Cells are suspended in 20 m*M* Tris–HCl pH 7.6 with DNase and disrupted by three passages through a French press at 6.9 MPa. The resulting extract is centrifuged at 12,000 *g* for 10 min at 4°C to remove cell debris. The supernatant is then centrifuged at 180,000 *g* for 90 min at 4°C to collect the cell membranes, which can be processed immediately or stored at −80°C. Membranes are first washed and homogenized by suspending them in 20 m*M* Tris–HCl pH 7.6 with 1 m*M* EDTA and DNase followed by ultracentrifugation at 180,000 *g* for 90 min at 4°C. The washed membranes are solubilized in 20 m*M* Tris–HCl at pH 7.6 with 2% (w/v) Zwittergent SB3–12 (SB3–12) in the presence of protease inhibitors. Solubilization is carried out overnight in an ice bath with gentle stirring, with the headspace of the glass vial filled with N_2 to avoid prolonged contact with O_2. The solubilized proteins are separated by ultracentrifugation at 180,000 *g* for 90 min

at 4°C, and the pellet can be used for a second solubilization using the same conditions. The extract with solubilized membrane proteins is loaded on a Q-Sepharose HP column (XK 26/10—GE Healthcare) equilibrated with buffer A (20 m*M* Tris–HCl at pH 7.6 plus 0.2% (w/v) SB3–12). The flow rate is 4 mL/min and a stepwise gradient of NaCl concentration is performed (0–350 m*M*, with 50 m*M* steps). Fractions eluted at different NaCl concentrations are concentrated in an Amicon stirred ultrafiltration cell with a 30 kDa cutoff membrane, where the ionic strength is also adjusted, if necessary. The total protein concentration is determined by the Bradford assay and an activity-stained native gel is used to identify those fractions having hydrogenase activity. The $[NiFeSe]_m$ hydrogenase elutes at around 300 m*M* NaCl.

The membrane-bound Ech and Coo hydrogenases of *D. vulgaris* Hildenborough are not detected during purification of the membrane extract: this can be due to their intrinsic instability, a characteristic of the family of multisubunit membrane [NiFe] hydrogenases related to Complex I (Hedderich, 2004), or to a low expression level (Valente et al., 2005).

A single step of ionic exchange chromatography is not sufficient to obtain pure protein, so the fraction of interest from the first chromatographic step is again loaded in a second Q-Sepharose HP column (XK 16/10—GE Healthcare) and the procedures described above are repeated. For the final polishing step, the fraction having activity expected for $[NiFeSe]_m$ hydrogenase is loaded onto a Q-resource column equilibrated with 20 m*M* Tris–HCl at pH 7.6 and 0.1% (w/v) *n*-dodecyl β-D-maltoside (DDM) or 0.2% SB3–12, and a stepwise NaCl gradient is performed (0–350 m*M*, with 50 m*M* steps). This column yields pure $[NiFeSe]_m$ hydrogenase as judged by the SDS-PAGE and activity-stained native gels. The fraction with pure enzyme is concentrated and the ionic strength is adjusted. It is stored in 20 m*M* Tris–HCl buffer pH 7.6 with 0.1% (w/v) DDM or 0.2% SB3–12.

2.3 Purification of the soluble form of the [NiFeSe] hydrogenase

The $[NiFeSe]_s$ hydrogenase can be purified either from the soluble extract obtained by washing the crude membranes (Valente et al., 2005) or from the solubilized membranes (Marques, Coelho, Pereira, & Matias, 2009). The purification of the soluble form follows the steps described above for the membrane form, with the exception that no detergent is used after the first column.

Another way to obtain the $[NiFeSe]_s$ hydrogenase is by incubating the membrane form with a commercial lipase (Valente et al., 2007). This procedure circumvents the low and nonreproducible yields obtained when the $[NiFeSe]_s$ hydrogenase is isolated directly from the membranes. The procedure consists of mixing 50 m*M* $[NiFeSe]_m$ hydrogenase with 5 mg of lipase, in a 20 m*M* Tris–HCl pH 8.0 buffer, at 37°C for 12 h: yields of almost 99% soluble $[NiFeSe]_s$ hydrogenase are obtained (Marques et al., 2013). It should be noted that the lipase acts here as a protease, similar to that which happens in vivo, cleaving off the first 11 residues from the large subunit (Valente et al., 2007).

3. Production of the recombinant *D. vulgaris* Hildenborough [NiFeSe] hydrogenase

3.1 Creation of the deletion mutant for the [NiFeSe] hydrogenase

The growth medium used when genetically manipulating *D. vulgaris* is the MOYLS4-rich medium (Zane, Yen, & Wall, 2010) with the following composition: 60 m*M* sodium lactate, 30 m*M* Na_2SO_4, 8 m*M* $MgCl_2$, 20 m*M* NH_4Cl, 0.6 m*M* $CaCl_2$, 2 m*M* phosphate (K_2HPO_4/NaH_2PO_4), 60 μ*M* $FeCl_2$, 120 μ*M* EDTA, 30 m*M* Tris (pH 7.4), 1 g/L yeast extract, 1 mL/L Thauers vitamin (Brandis & Thauer, 1981), and 6 mL/L trace elements solution with the pH adjusted to 7.2, plus 0.001% (w/v) resazurin (as oxygen indicator). The trace elements solution contains the following concentrations of salts: 2.5 m*M* $MnCl_2{\cdot}4H_2O$, 1.26 m*M* $CoCl_2{\cdot}6H_2O$, 1.47 m*M* $ZnCl_2$, 210 μ*M* $Na_2MoO_4{\cdot}2H_2O$, 320 μ*M* H_3BO_3, 380 μ*M* $NiSO_4{\cdot}2H_2O$, 11.7 μ*M* $CuCl_2{\cdot}2H_2O$, 35 μ*M* $Na_2SeO_3{\cdot}5H_2O$, and 24 μ*M* $Na_2WO_4{\cdot}2H_2O$.

A mutant strain for *hys*A and *hys*B genes (coding for the large and small subunits of [NiFeSe] hydrogenase, respectively) was produced by double homologous recombination in *D. vulgaris* Hildenborough, based on the marker exchange approach as previously described (Keller, Wall, & Chhabra, 2011). For the *hys*AB deletion, the plasmid pMOIP01 was produced by sequence ligation-independent cloning (SLIC) (Li & Elledge, 2007), using the following PCR amplified segments: 1055 bp upstream of *hys*AB (hysAB Up Fw—GCCTTTTGCTGGCCTTTTGCTCACAT GGACAAGGATGAGCCCGTTGTGAA and hysAB Up Rev—AAGACTGTAGCCGTACCTCGAATCTATGC AGTGCCAGCCAA

TAGAGTGAA), 885 bp downstream of hysAB (hysAB Dwn Fw—AATCCGCTCACTAAGTTCATAGACCGGACGCCCATGAT GTTAGGGTTCCAA and *hys*AB Dwn Rev—CGAGGCATTTC TGTCCTGGCTGGGCGTACGCATTACGCACGTATCAT); the kanamycin resistance gene, taken from the pSC27 plasmid (Keller, Bender, & Wall, 2009) (Kan Fw—TAGATTCGAGGTACGGCT ACAGTCTTACGGTCACAAACAGGTACGCCCCCAGAGTC and Kan Rev—CGGTCTATGAACTTAGTGAGCGGATTTCTCGTGTA GCCGATGCAGTGAGGTAGCTTGCAG); spectinomycin resistance gene; and the pUC ori portion taken from pMO719 background (Keller et al., 2009). The products from the amplifications were transformed into *E. coli* α-select Silver Efficiency (Bioline), and successful transformants were isolated on lysogeny broth (LB)-agar medium containing 50 μg/mL kanamycin and 100 μg/mL spectinomycin. Correct isolates were identified by the expected PCR amplicons from the plasmid constructs and also by sequencing. The pMOIP01 plasmid was electroporated into *D. vulgaris* Hildenborough with the following parameters: 1500 V, 250 Ω, and 25 μF, from which the deletion strain for *hys*AB, IPAR01 (Δ*hys*AB), was obtained, by selection with MOYLS4 medium containing 400 μg/mL geneticin (Keller et al., 2011). The deletion of *hys*AB was confirmed by Southern blot using an upstream fragment of the *hys*AB gene as probe.

3.2 Expression vector and complemented strain for [NiFeSe] hydrogenase expression

To produce the recombinant soluble form of [NiFeSe] hydrogenase an expression vector was constructed encoding *hys*B followed by a Strep-tag and *hys*A, lacking the codons for the first 11 amino acid residues. To create this vector, two segments were amplified by PCR: the *hys*B gene (HysB Fw—AGGTTGGGAAGCCCTGCAATGCAGTCCCAGGAGGTACC ATATGAGTCTCACAAGGCGTGATTTCGTC and HysB Rev— TTTTTCGAACTGCGGGTGGCTCCACATGATAT CCTCCTGA AGCGACTGACGG) and the Strep-tag in the N-terminal of *hys*A gene (HysA Fw—TGGAGCCACCCGCAGTTCGAAAAAGGGGCCACCG GCAGGACGACCATC and HysA Rev—GATCGTGATCCCCTGC GCCATCAGATCCTTGGCTCGCGGCCCCTCCCCTTCATGAT); and then added into pMO9075 background shuttle plasmid (Keller et al., 2009) via SLIC, creating the pMOIP03 plasmid. The amplification products were transformed into *E. coli* α-select Silver Efficiency, and cells were plated on LB agar with 100 μg/mL spectinomycin. The correct plasmid construct was screened by colony PCR and later confirmed by sequencing. In the

pMO9075 vector plasmid, the *hysA*B gene remains under the control of the Km^R gene-*aph(3′)-II* promoter, which is known to be constitutively expressed in *D. vulgaris* (Keller et al., 2009). The pMOIP03 vector was successfully introduced in the deletion strain IPAR01 by electroporation, with the following parameters: 1250 V, 250 Ω, 25 μF. The complemented strain for HysAB was grown in MOYLS4 medium containing 400 μg/mL geneticin and 100 μg/mL spectinomycin. The plasmid was confirmed by PCR amplification of the insert and also by sequencing. Western-Blot against the Strep-Tactin AP (IBA) antibody was performed to confirm expression.

3.3 Site-directed mutagenesis of the [NiFeSe] hydrogenase

For site-directed mutagenesis, the plasmid pMOIP03 carrying a *hysA*$_{Strep}$*hys*B fragment is used as a template. The amino acid exchange is carried out using the NZYMutagenesis kit (Nzytech), with mutagenic primers designed on the basis of the codon usage in *D. vulgaris* Hildenborough. For propagation, the mutagenic plasmid is transformed into *E. coli* Nzy5α (Nzytech), which is transferred to 1 mL LB medium for growth at 37°C, under aerobic conditions for 1 h. Cells are plated in LB-agar medium containing 100 μg/mL spectinomycin, and isolated colonies are grown on LB medium. The plasmid is extracted by Miniprep and sequenced to check for the correct amino acid exchange. The plasmid pMOIP03 carrying the correct mutation is then electroporated aerobically into the deletion IPAR01 strain using the Gene Pulser XCell (Bio-Rad), with the following parameters: 1250 V, 250 Ω, 25 μF. Electroporated cells are transferred to 1 mL of MOYLS4 medium and left to recover anaerobically overnight at 37°C. About 50–100 μL of these cells are plated, with molten MOYLS4 medium containing 400 μg/mL geneticin and 100 μg/mL spectinomycin poured over the cells and swirled. Once solidified, plates are inverted and placed in an airtight rectangular jar (Mitsubishi Gas Chemical Co., Inc., Japan) with an oxygen indicator strip (Biomérieux) and GenBox Anaer (Biomérieux) to absorb traces of O_2. The plates are incubated in a growth chamber at 37°C, between 2 and 5 days until *D. vulgaris* Hildenborough colonies appear (Fig. 4). The colonies are selected with a sterile toothpick and inserted into MOYLS4 liquid medium with 100 μg/mL spectinomycin. The first *D. vulgaris* Hildenborough [NiFeSe] hydrogenase variant was recently reported, where the Sec489 residue was exchanged for a Cys, transforming the active site of the [NiFeSe] hydrogenase into that of a [NiFe] hydrogenase (Marques et al., 2017).

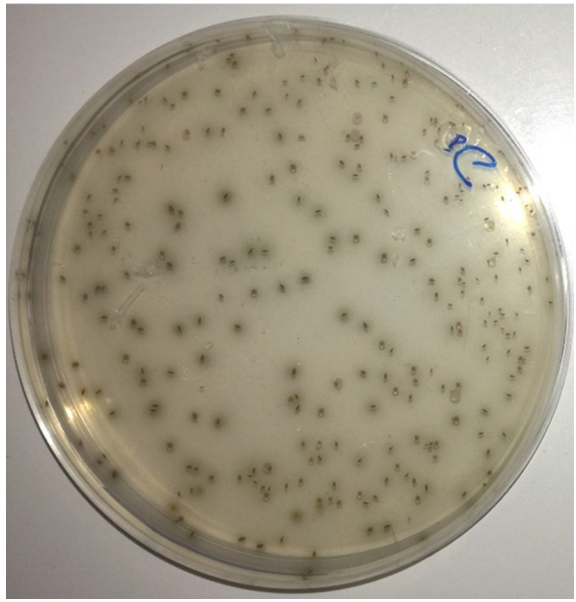

Fig. 4 Colonies of *D. vulgaris* Hildenborough plated in MOYLS4 medium.

3.4 Purification of the recombinant [NiFeSe] hydrogenase

Cells are suspended in 20 m*M* Tris–HCl pH 7.6 with DNase and disrupted by three passages through a French press at 6.9 MPa. The resulting extract is centrifuged at 12,000 *g* for 10 min at 4°C to remove cell debris. The supernatant is then centrifuged at 180,000 *g* for 90 min at 4°C to separate membranes from the soluble fraction. The soluble fraction is loaded onto a Q-Sepharose HP column (XK 26/10—GE Healthcare) equilibrated with 20 m*M* Tris–HCl pH 7.6, then a stepwise NaCl gradient is performed (0–350 m*M*, with 50 m*M* steps), whereupon fractions with $[NiFeSe]_r$ hydrogenase activity usually elute between 250 and 300 m*M* NaCl. The combined fractions are concentrated and the ionic strength adjusted using an Amicon stirred ultrafiltration cell with a 30 kDa cutoff membrane. Affinity chromatography is then performed by loading the fraction onto a gravity column containing Strep-Tactin resin (IBA Lifesciences) equilibrated with 100 m*M* Tris–HCl pH 8.0, 150 m*M* NaCl (buffer W). After five washing steps with buffer W, the recombinant protein was eluted with buffer W plus 2.5 m*M* desthiobiotin. This column yields pure [NiFeSe] hydrogenase as judged by SDS-PAGE. Protein concentration is determined based on $\varepsilon_{410} = 48{,}000\ M^{-1}\ cm^{-1}$, using the protein molecular mass of 88,000 Da.

4. Hydrogenase activities

The steady-state activity of the [NiFeSe] hydrogenase is routinely quantified by measuring the rates of hydrogen oxidation and proton reduction with artificial redox dyes. We use methyl viologen (MV) ($E = -449$ mV at all pH values) both as electron donor for H_2 production and as electron acceptor for H_2 oxidation. The natural physiological partner, TpIc_3, can also be used as electron acceptor or donor to assay hydrogenase activity in vitro (Valente et al., 2005). The H_2 oxidation activity can also be assessed qualitatively by activity-stained native gels.

The H/D isotope exchange activity measured by membrane-inlet mass spectrometry shows the reversibility of the [NiFeSe] hydrogenase catalytic function (Fig. 5). It is performed in the absence of a redox partner. Thus, no intermolecular electron transfer takes place; only H_2 cleavage/formation and proton exchange with the solution are involved during this catalytic process (Vignais, 2005).

Oriented immobilization of the [NiFeSe] hydrogenase on electrodes allows measuring its H_2 oxidation/production activities by electrochemical methods. Correct immobilization of the enzyme allows direct electron transfer with the electrode, thus avoiding the use of redox dyes as electron donors or acceptors (Rüdiger et al., 2010). The redox potential applied on the electrode drives the electrocatalytic process toward either proton reduction or H_2 oxidation, while the current is proportional to the enzymatic activity (Vincent, Parkin, & Armstrong, 2007). Benchmark H_2 oxidizing currents of $1.7\,mA\,cm^{-2}$, with bioanodes based on the *D. vulgaris* Hildenborough [NiFeSe] hydrogenase immobilized in a viologen-modified hydrogel, were recently achieved (Ruff et al., 2017, 2018).

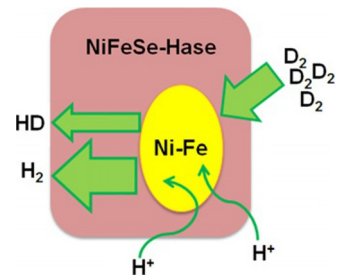

Fig. 5 Scheme depicting the H/D isotope exchange activity of [NiFeSe] hydrogenase in D_2/H_2O.

4.1 H_2 evolution and uptake with artificial mediators

4.1.1 H_2 evolution assay

The rate of H_2 evolution is obtained by assaying with gas chromatography (GC) in a Trace GC Ultra (Thermo Scientific) equipped with a thermal conductivity detector (TCD), using a MolSieve 5A 80/100 column (Althech) and N_2 as carrier gas. The assay is performed in a gas-tight screwcap vial containing 1 mL of 50 m*M* Tris–HCl buffer at pH 7 plus 1 m*M* MV, 15 m*M* sodium dithionite, 0.5 mg/mL bovine serum albumin, and 9 mL volume headspace filled with N_2. The reaction is initiated by adding to the vial 10 μL of approximately 9 n*M* enzyme with a gas-tight syringe. Dithionite-reduced MV is the electron donor for the [NiFeSe] hydrogenase. This reaction mixture is incubated in a shaker at 37°C for 10 min and a headspace sample is injected into the GC every 5–10 min. The GC measurements are calibrated by controlled injections of H_2 under identical liquid and gas volume headspaces. One unit of enzyme is defined as the amount of hydrogenase evolving 1 μmol of H_2/min. The purified $[NiFeSe]_r$ Hydrogenase exhibits a H_2-production activity of around 5650±260 U/mg ($8280 \pm 380\,s^{-1}$).

4.1.2 H_2 uptake assay

The rate of H_2 uptake (oxidation) is measured spectrophotometrically in a Coy anaerobic chamber (95% N_2, 5% H_2), using a UV-1800 Shimadzu spectrophotometer. The enzyme is first activated with 0.5 bar H_2 at room temperature for approximately 30 min in an anaerobic vial containing 1 mL of 50 m*M* Tris–HCl buffer at pH 8 and 1 m*M* MV. Inside the anaerobic chamber, the reaction is initiated by adding 10 μL of approximately 25 n*M* enzyme to a cuvette containing 1 mL of H_2-saturated 50 m*M* Tris–HCl buffer at pH 8 and 2 m*M* MV, with constant stirring. The H_2 oxidation activity is measured from the reduction of MV, following the MV color change rate at 604 nm ($\varepsilon = 13.6\,mM^{-1}\,cm^{-1}$) at 30°C, according to the reaction: $H_2 + 2MV^{+2} \rightarrow 2H^+ + 2MV^+$. One unit of enzyme is defined as the amount of hydrogenase reducing 2 μmol of MV per minute, which is equivalent to 1 μmol H_2 oxidized per minute. The $[NiFeSe]_r$ hydrogenase exhibits an H_2 uptake activity of around 3310 ± 180 U/mg (4450 ± $220\,s^{-1}$).

4.1.3 Activity-stained native gels

For a qualitative assessment of the hydrogenase activity, either in crude cell extracts or in the purification fractions, activity staining is performed using

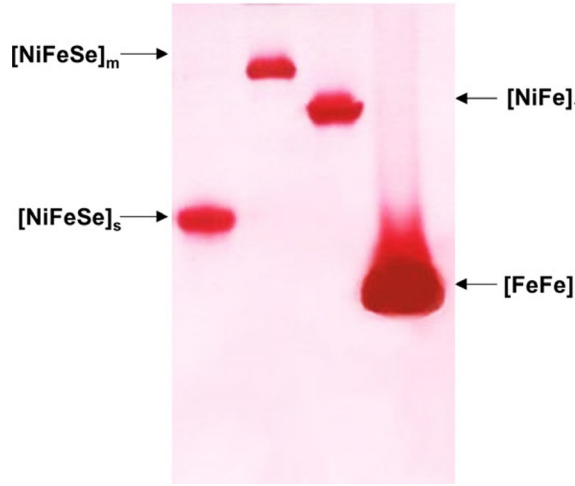

Fig. 6 Activity-stained native gel for hydrogenase activity of pure protein samples isolated from *D. vulgaris* Hildenborough. The $[NiFeSe]_r$ hydrogenase, not represented here, migrates on the gel with the same profile as the $[NiFeSe]_s$ hydrogenase.

native polyacrylamide gel electrophoresis (Fig. 6). The band intensity is related to the H_2 uptake activity, since the enzyme will oxidize H_2 and transfer the electrons to MV, giving rise to a blue band on the gel. Activity-stained gels are routinely used throughout the protein purification process, to identify fractions with hydrogenase activity as well as to screen rapidly for [NiFeSe] hydrogenase variants with significant differences in H_2 oxidation activity, based on the intensity of the bands.

Samples of 50–200 µg total protein from either soluble fractions or fractions taken from the ionic exchange chromatography are run in a 7.5% (v/v) polyacrylamide gel containing 0.1% (v/v) Triton X-100. Detergent is important for the membrane-associated hydrogenases to run properly since its absence results in band streaking. The gel is transferred to 50 mL of an N_2-saturated solution of 50 m*M* Tris–HCl pH 7.6 containing 0.5 m*M* MV and then incubated under 0.5 bar H_2. Once blue bands are well developed, they are fixed by adding 10 m*M* 2,3,5-triphenyltetrazolium chloride which is reduced by MV to give a permanent oxygen-insensitive red stain.

4.2 H/D isotope exchange activity

The H/D isotope exchange activity of the hydrogenase is measured in a thermostated, magnetically stirred 37°C reactor that is connected via a 14 µm Teflon membrane to a mass spectrometer (Pfeiffer Prisma)

(Gutiérrez-Sanz, Marques, Baltazar, et al., 2013). The output signal of the spectrometer for mass values 2 and 4 is calibrated by saturating buffered solutions with 100% H_2 and 20% D_2 in 80% Ar, respectively, which have been passed through an oxygen filter (Varian) before entering the reactor. The output signal is proportional to the partial pressure of the corresponding gas in the reaction vessel (Vignais, 2005). Calibration for the single exchange product of the enzymatic reaction (HD) is determined from the average values measured for H_2 and D_2.

Generally, the exchange activity is measured in 10 mL of buffered H_2O solution purged with 20% D_2 in Ar. After reaching a plateau value for mass 4, the reactor lid is closed while excluding the gas phase in the reactor. The enzymatic reaction is initiated by adding sequentially, through a rubber septum with gas-tight syringes, 100 μL of 1% DDM, 1 μL of 1 *M* sodium dithionite to eliminate residual oxygen, and typically 25 μL of 0.1 μ*M* hydrogenase. During the measurement, masses 2, 3, and 4 are scanned at a rate of 1 amu/s. The initial rates of H_2 and HD production are calculated from the difference in the slopes after and before enzyme addition (Gutiérrez-Sanz, Marques, Baltazar, et al., 2013). Alternatively, the isotope exchange activity can be measured by saturating a buffered D_2O solution with H_2. In this case HD and D_2 production rates are measured by monitoring the evolution of masses 3 and 4, respectively. In this case the hydrogenase sample needs to be preincubated overnight in the D_2O-buffered solution in order to convert exchangeable protons to deuterons (Gutiérrez-Sanz, Marques, Baltazar, et al., 2013).

4.3 Electrocatalytic H_2 production and oxidation

Covalent immobilization of the [NiFeSe] hydrogenase on a gold electrode modified with a 4-aminothiophenol (4-ATP) self-assembled monolayer (SAM) enables measuring its electrocatalytic H_2 oxidation/production activity to be measured by direct electron transfer. The 4-ATP SAM is formed by immersing a clean Au electrode in a 5 m*M* solution of 4-ATP in ethanol for 18 h at room temperature. After rinsing, the Au electrode surface is covered by 6 μL of 27 μ*M* hydrogenase in 10 m*M* MES, pH 6.5 for 30 min then, in a second step, 5.5 μL of 14 m*M* *N*-(3-dimethylaminopropyl)-*N*′-ethylcarbodiimide hydrochloride (EDC) and 4.5 μL of 21 m*M* *N*-hydroxysuccinimide, in the same buffer solution, are added in order to form amide bonds between the enzyme and the 4-ATP SAM on the electrode. The mixture is left to react for 90 min, then the modified Au surface is washed for 5 min in 0.1 *M* phosphate, pH 7.0, 0.25 *M* KCl

buffer solution with stirring to remove noncovalently bound hydrogenase (Rüdiger et al., 2010). Electrocatalytic experiments are controlled by an Autolab potentiostat and measured in a three-electrode glass cell equipped with a platinum wire counter-electrode and a saturated calomel reference electrode separated from the main compartment in a sidearm connected by a Luggin capillary. The electrochemical cell is surrounded by a water jacket for controlling the temperature at 40°C. The gold working electrode is connected to an MSR electrode rotator (Pine Instruments). The electrocatalytic H_2 oxidation activity is measured by chronoamperometry at −0.25 V vs NHE, under 1 atm H_2 at an electrode rotation rate of 2500 rpm, whereas the H_2 production is measured at −0.45 V vs NHE under 1 atm N_2 (Rüdiger et al., 2010). The membrane form of the [NiFeSe] hydrogenase can be immobilized on Au gold electrodes modified with a phospholipid bilayer by using the enzyme's hydrophobic tail as an anchor to the supported biomimetic membrane. Two different orientations of the membrane-bound hydrogenase on the electrode are possible: (i) the enzyme is inserted via its hydrophobic tail onto a phospholipid bilayer supported on a 4-ATP-modified Au electrode with its 4Fe4S distal cluster facing the bulk solution; (ii) the enzyme is covalently bound to the 4-ATP-Au with its 4Fe4S distal cluster facing the electrode and a phospholipid bilayer is formed on top of the hydrogenase monolayer using the hydrophobic tail as scaffold (Gutiérrez-Sánchez et al., 2011). The first configuration is obtained by incubating the 4-ATP-Au electrode in a 0.6 mg/mL liposome suspension (300 nm diameter) from *E. coli* polar extract in 10 m*M* MES buffer at pH 5 for 45 min at room temperature. After rinsing carefully with MES buffer 10 m*M* at pH 7, the electrode is incubated in 27 μ*M* $[NiFeSe]_m$ hydrogenase in pH 6.0 MES buffer and 48 mg of dry CALBIOSORB adsorbent is added to the solution for 1.5 h to remove the detergent present in the hydrogenase solution (Gutiérrez-Sánchez et al., 2011). The second configuration is obtained in two steps by first immobilizing covalently on the 4-ATP-Au the $[NiFeSe]_m$ hydrogenase as described above but in the presence of 0.1% DDM. The second step involves incubating the hydrogenase-modified electrode in the liposomes suspension in the presence of CALBIOSORB adsorbent for 90 min (Gutiérrez-Sanz et al., 2013). It has been shown that the hydrogenase immobilized on electrodes in the latter configuration is able to create a proton gradient across the biomimetic membrane upon electrocatalytic H_2 oxidation (Gutiérrez-Sanz et al., 2015) and to induce ATP synthesis when an ATP synthase is incorporated in the phospholipid bilayer (Gutiérrez-Sanz et al., 2016).

4.4 Photocatalytic H_2 production

The [NiFeSe] hydrogenase can produce H_2 when combined with appropriate visible light-absorbing semiconductors such as In_2S_3 (Tapia et al., 2016). The In_2S_3 should be presented as a polycrystalline powder with a controlled pore size around 15–20 nm in diameter, suitable for hosting the enzyme and allowing electron transfer, and it is synthesized by a hydrothermal procedure as follows. A Pyrex beaker located inside a Teflon-lined steel high-pressure reactor is filled with 50 mL aqueous solution containing 148 m*M* $InCl_3$, 178 m*M* thiourea, and 80 μL HCl 37%, and the mixture is left to react at 162°C for 2 days (Lucena, Aguilera, Palacios, Wahnón, & Conesa, 2008). Afterward, the material is cleaned by three centrifugation-resuspension cycles in distilled water and another one in ethanol. Finally, the material is dried for 12 h at 333 K.

The [NiFeSe] hydrogenase is incubated for 6 h with the In_2S_3 nanoparticles to adsorb the enzyme on the surface. This process is performed at 4°C by mixing 0.26 pmol of hydrogenase with 22.1 μmol of In_2S_3 in 10 mL of a pH 7.0 solution containing 50 m*M* Tris–HCl and 0.2 *M* Na_2SO_3 (Tapia et al., 2016). The sample is then transferred to a glass reactor vessel connected to a mass spectrometer through a gas-permeable Teflon membrane, taking care to avoid a gas phase inside the reaction chamber. The [NiFeSe] hydrogenase is preactivated by bubbling a mixture of 1:4 H_2/Ar for 10 min followed by pure Ar to remove all the H_2 from the reactor. Upon irradiating the activated sample with light from a 450 W Xe lamp solar simulator, H_2 is produced, the rate being measured by mass spectrometry, monitoring mass = 2.

5. Structure determination of *D. vulgaris* Hildenborough [NiFeSe] hydrogenase by X-ray crystallography

5.1 Crystallization

The soluble forms of the [NiFeSe] hydrogenase (either native or recombinant) are crystallized aerobically at 20°C using the sitting drop vapor diffusion method, using microbridges in 24-well plates (Hampton Research). Crystallization drops are prepared by mixing 1 or 2 μL of pure protein having a concentration between 80 and 114 μ*M*, with an equal volume of reservoir solution containing ca. 20% PEG 1500 (w/v), 0.1 m*M* Tris–HCl, pH 7. The exact percentage of PEG 1500 varies somewhat depending on the protein batch, and some optimization is usually required to obtain the best quality crystals. Drops are equilibrated against 500 μL of

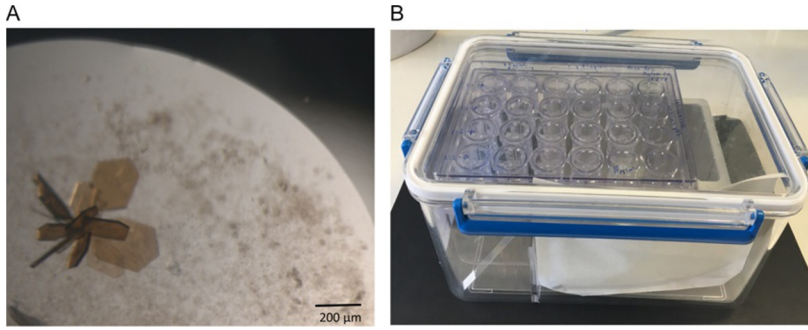

Fig. 7 (A) Crystals of the $[NiFeSe]_r$ hydrogenase. (B) Crystallization plate inside an airtight jar to allow crystal growth under anaerobic conditions. An oxygen indicator strip and GenBox Anaer are placed inside the jar.

reservoir solution. Brown monoclinic blocks, with dimensions varying from 100 to 500 µm, grow over 4–6 days (Fig. 7A). Crystals are prepared for data collection with the reservoir solution adjusted to include 10% (v/v) glycerol and flash-cooled in liquid nitrogen or under a nitrogen gas stream at 100 K. Recombinant [NiFeSe] hydrogenase and variants usually crystallize in the monoclinic space group *C*2 with one molecule in the asymmetric unit, but the as-isolated native soluble enzyme was crystallized in monoclinic space group $P2_1$: crystallization occasionally occurs in other space groups.

For anaerobic crystallization, the procedure used is the same as described above except that it is carried out in a Coy anaerobic chamber (95% N_2, 5% H_2). All plastic materials and solutions are degassed and introduced to the chamber 1 day in advance. A 24-well crystallization plate with the crystallization drops is kept in an airtight rectangular jar (Mitsubishi Gas Chemical Co., Inc., Japan) with an oxygen indicator strip (Biomérieux) and GenBox Anaer (Biomérieux), outside the anaerobic chamber in a 20°C room (Fig. 7B). Harvesting crystals under anaerobic conditions is achieved by filling a container with argon, and the crystal plate and stereoscopic microscope are placed in this container.

The $[NiFeSe]_m$ hydrogenase has not been crystallized to date, despite screening of multiple crystallization conditions at the 100 nL scale using a robot.

5.2 Data collection and structure determination

Crystals of $[NiFeSe]_r$ hydrogenase usually display good diffraction quality on a home X-ray source (either a rotating anode X-ray generator or a microsource) coupled to a mirror system and a CCD detector, yielding diffraction

data to a resolution of ca. 1.5 Å. The use of a four-circle diffractometer leads to very complete diffraction data with high multiplicity, obviating the cusp that can result from measuring a monoclinic crystal on a one-circle goniometer. Likewise, modern detectors and data collection software at synchrotron sources yield nearly 100% complete diffraction data to a resolution approaching 1 Å, with the added benefit of wavelength selection at some beamlines, which is very important to validate the structure of the active site, in particular the bimetallic NiFe and the position of the Se atom in the selenocysteine ligand.

The diffraction quality displayed by the first crystals of the as-isolated soluble form of [NiFeSe] hydrogenase was relatively poor. The first data set was obtained *in-house* to a resolution of 2.4 Å, and although a homologous structure from *Dm. baculatum* [NiFeSe] hydrogenase was already known (PDB 1CC1; Garcin et al., 1999) and a clear solution could be obtained by the molecular replacement method, the electron-density maps were not of sufficiently good quality to rebuild several regions in the structure (Marques et al., 2009).

Therefore, the crystal structure of $[NiFeSe]_s$ hydrogenase from *D. vulgaris* Hildenborough was determined at 2 Å resolution from a crystal of the as-isolated soluble form, using the Multiple Wavelength Anomalous Dispersion Method at the Fe K-edge (Marques et al., 2010) from data measured at Diamond Light Source beamline I04 (Didcot, UK) (Fig. 8). The peak and inflection point wavelengths were chosen to maximize the anomalous and dispersive signals with CHOOCH (Evans & Pettifer, 2001) from an X-ray fluorescence scan near the Fe K-edge, and the remote wavelength was chosen around 1 Å to minimize absorption effects and maximize dispersive differences during phasing. The diffraction images for the three data sets were processed with XDS (Kabsch, 1993).

The as-isolated soluble form of $[NiFeSe]_s$ hydrogenase from *D. vulgaris* Hildenborough crystallized in space group $P2_1$ with one heterodimer in the asymmetric unit; therefore, 14 Fe sites were expected (1 in the NiFe active site, 12 in the three 4Fe4S clusters, and 1 bound to the C-terminal region of the large subunit). Using the HKL2MAP graphical interface (Pape & Schneider, 2004) and the SHELXC/D/E program suite (Schneider & Sheldrick, 2002; Sheldrick, 2002, 2010) the data set was scaled and analyzed with SHELXC, the Fe-atom substructure was determined with SHELXD, and the phase problem solved with SHELXE. However, although a good solution for the Fe-atom substructure was obtained with SHELXD, a clear and unequivocal discrimination between the correct and inverted

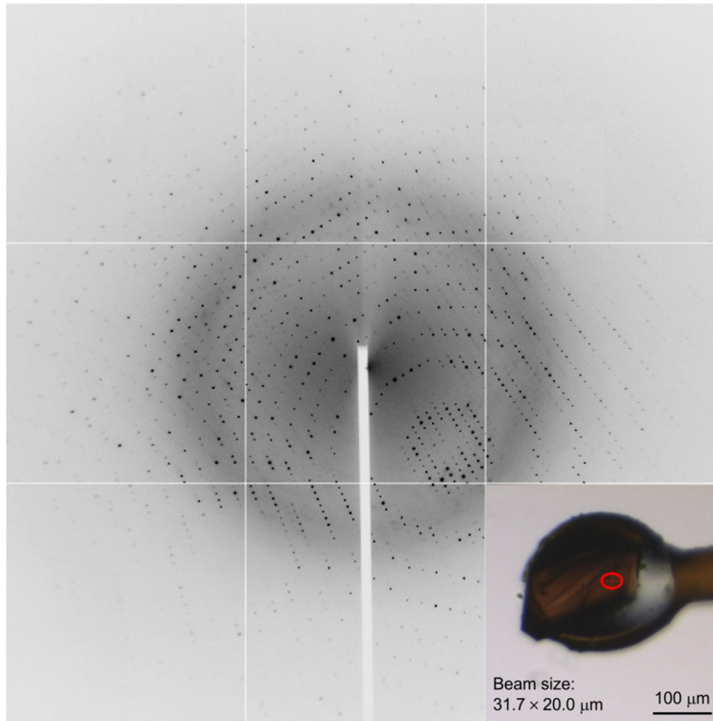

Fig. 8 Diffraction image from the data set measured at the Fe peak wavelength (1.7244 Å) used in the structure determination of *D. vulgaris* [NiFeSe] hydrogenase. The *inset* shows a typical cryocooled crystal used for diffraction data measurements at the Diamond Light Source.

substructures could not be obtained with SHELXE and the electron-density maps could not be interpreted. Improved phases were obtained using the maximum-likelihood heavy-atom parameter refinement in SHARP (Bricogne, Vonrhein, Flensburg, Schiltz, & Paciorek, 2003) and a subsequent optimizing density modification procedure using SOLOMON (Abrahams & Leslie, 1996) and DM (Cowtan, 1994). Automated model building with ARP/wARP (Perrakis, Morris, & Lamzin, 1999) produced a near-complete model for the protein chains of both subunits (except for a few disordered N-terminal residues). Prior to structure refinement, the 4Fe4S clusters and the NiFe cofactors were modeled with COOT (Emsley, Lohkamp, Scott, & Cowtan, 2010).

Subsequent crystal structures of the as-isolated soluble or recombinant forms of [NiFeSe] hydrogenase from *D. vulgaris* Hildenborough were determined by the Molecular Replacement Method with PHASER

(McCoy, 2006) using an earlier crystal structure as phasing model, with separate rotation/translation calculations for each subunit, and usually omitting the metal cofactors. High-resolution diffraction data for these structural studies have been measured at several European synchrotron sources: ESRF (Grenoble, France), SLS (Villigen, Switzerland), ALBA (Cerdanyola del Vallès, Spain), and DLS (Didcot, UK).

5.3 Structure refinement

The first crystal structure of the as-isolated soluble form of [NiFeSe] hydrogenase from *D. vulgaris* Hildenborough was refined against the 2.04 Å peak data measured at DLS using a maximum-likelihood procedure with REFMAC (Murshudov et al., 2011) as implemented in the CCP4i graphics user interface (Potterton, Briggs, Turkenburg, & Dodson, 2003). Prior to refinement, a random 5% sample of the reflection data was flagged for cross-validation using R-free (Brünger, 1992). Improved atomic displacement parameters at this resolution were obtained using a simple TLS (translation–libration–screw) rigid body model (Winn, Isupov, & Murshudov, 2001) where each of the two subunits (including its respective cofactors) was treated as a rigid body. During refinement, the structure was regularly inspected and corrected against σ_A-weighted $2|F_o|-|F_c|$ and $|F_o|-|F_c|$ electron-density maps using COOT. The map coefficients were calculated by REFMAC at the end of each refinement procedure. In this crystal structure, electron density for the aliphatic chains of four sulfobetaine 3–12 detergent molecules used in the purification was observed in two hydrophobic pockets open to the solvent and the visible atoms were included in the refinement. Solvent molecules were located with ARP/wARP and by inspection of σ_A-weighted $2|F_o|-|F_c|$ and $|F_o|-|F_c|$ electron-density maps, and included in the refinement.

Refinements of subsequent crystal structures of both as-isolated soluble and recombinant forms of [NiFeSe] hydrogenase from *D. vulgaris* Hildenborough were carried out using PHENIX (Adams et al., 2010). Although considerably slower than REFMAC, PHENIX allows for the refinement of occupation factors, which in the case of these structures is very important to elucidate the fine structural details of the active site. Since most datasets have been measured just above the K-absorption edge of selenium, the Se atom in selenocysteine displays significant anomalous dispersion properties ($\Delta f' \sim -4$ e^- and $\Delta f'' \sim 3.5$ e^-) and anomalous refinement is used, increasing the number of experimental data and allowing the direct

calculation of anomalous difference maps, which is very useful for validating structural changes in the active site and proximal 4Fe4S cluster. In all refinements, hydrogen atoms are included at calculated positions with REFMAC or the READYSET tool in PHENIX. At intermediate resolutions (up to ca. 1.5 Å) a TLS refinement of the atomic displacement parameters is followed by refinement of individual isotropic atomic displacement parameters for all nonhydrogen atoms. The TLS rigid bodies are chosen by submitting a previously refined structure with isotropic atomic displacement parameters to the TLS Motion Determination (TLSMD) server (Painter & Merritt, 2006) or by using the internal PHENIX tool. At higher resolutions, anisotropic refinement of atomic displacement parameters for all nonhydrogen atoms is undertaken. Solvent molecules can be added automatically during the refinement process in PHENIX or by inspection of the σ_A-weighted $2|F_o|-|F_c|$ and $|F_o|-|F_c|$ electron-density maps produced at the end of each refinement calculation.

6. *D. vulgaris* Hildenborough [NiFeSe] hydrogenase biophysical characterization

6.1 Infrared spectroscopy

The different redox states of the bimetallic active site of the hydrogenase can be studied by (Fourier-transform infrared spectroscopy) FTIR because its CO and CN^- ligands absorb infrared radiation and the vibrational frequencies of their bands are sensitive to changes in electron density at the active site (De Lacey, Fernández, Rousset, & Cammack, 2007). The FTIR-spectroelectrochemical experiments on [NiFeSe] hydrogenases are performed in a cell with an 8 μm path length described by Moss, Nabedryk, Breton, and Mantele (1990). For these measurements 10 μL of hydrogenase solution having a concentration of at least 0.8 m*M* in buffered solution with 0.2 *M* KCl is required. The sample must contain, in addition, a mixture of redox mediators, 0.05 m*M* in each case, the redox potentials of which span the range 0 to −450 mV vs NHE, in order to attain rapid equilibration with the electrode potential. The redox potential of the cell is controlled with a BAS CV-27 potentiostat and measured with a Fluke 77 multimeter. The temperature of the cell is controlled at 25°C with a thermostat. Spectra are recorded in an FTIR spectrometer with a Mercury Cadmium Telluride (MCT) detector and purged with a CO_2- and H_2O-free atmosphere (Fig. 9). The FTIR spectra are averaged from 1024 scans

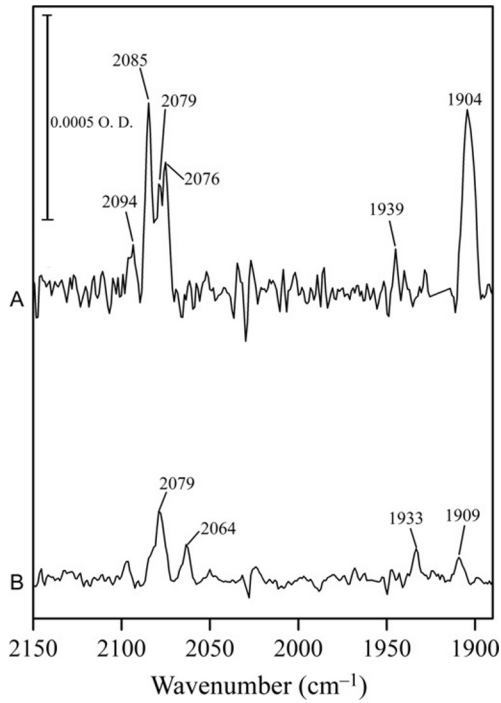

Fig. 9 FTIR spectra of *D. vulgaris* Hildenborough [NiFeSe] hydrogenase active site as isolated aerobically (A) and after reduction with 1 atm of H_2 (B).

and the spectral resolution is $2\,cm^{-1}$ (De Lacey, Gutiérrez-Sánchez, Fernández, Pacheco, & Pereira, 2008).

Surface-enhanced infrared absorption spectroscopy is a nonconventional infrared spectroscopy technique that is based on the surface enhancement effect of infrared absorption in rough (at the nanoscale) metals. It can be used for studying the [NiFeSe] hydrogenase immobilized on a 4-ATP-Au electrode. For this type of measurement, a trapezium-shaped silicon ATR-IR element covered with a nanostructured SEIRA Au film formed by electroless deposition is used. All spectra are recorded within a spectral window of $4000–1000\,cm^{-1}$ and with a resolution of $2\,cm^{-1}$ using an FTIR spectrometer with an MCT detector. For each spectrum, 620 scans are accumulated (Gutiérrez-Sanz, Marques, Pereira, et al., 2013).

6.2 Atomic force microscopy

The atomic force microscope (AFM) images the topography of modified surfaces describing the height and density of the proteins on the surface as

well as the integrity and smoothness of a lipid bilayer. Measurements are performed using a flat substrate that consists of 200 nm gold evaporated over 1–4 nm chromium prepared on borosilicate glass (Metallhandel Schröder GMBH). Substrates are cleaned with "piranha" solution followed by exhaustive rinsing with Milli Q water and a final rinse with ethanol/water (2:1): they are then annealed to an orange glow for a few seconds in a propane flame (the heating is repeated five times). This treatment produces Au (111) grains of a few μm radius with atomically flat surfaces, suitable for AFM characterization. This atomically flat gold surface is then treated as described above (Section 4.3) to form the 4-ATP SAM and to covalently attach the enzyme for direct electron transfer. The protocol to form the bilayer on the gold substrate is also the same as that mentioned in Section 4.3. Imaging is carried out using either a Nanotec microscope operating in jumping mode or an Agilent Technologies (Santa Clara, CA) 5500 microscope used in tapping mode. Measurements were always made under liquid conditions in PBS buffer at room temperature using Olympus rectangular silicon nitride cantilevers (RC800PSA, $200 \times 20\,\mu m$) with a spring constant of 0.05–0.10 N/m, an estimated tip radius of 20 nm, and a resonance frequency in the liquid cell of approximately 27 kHz. Scanning rates are kept close to 1 Hz. Images contain 512×512 pixels and are first-order flattened using Picoimage software from Agilent or WSxM software from Nanotec Electronica (Gutiérrez-Sánchez et al., 2011; Rüdiger et al., 2010).

6.3 Quartz crystal microbalance

A quartz crystal microbalance (QCM) measures, in real time, the amount of material adsorbed on a surface. It is a useful instrument to aid in the sequential modification of electrodes described in Section 4.3 to measure electrocatalytic H_2 production and oxidation coupled to the creation of a proton gradient across a lipid membrane used to synthesize ATP. QCM measurements are used to verify the formation of a lipid bilayer containing ATPase synthase. Experiments are performed with 5 MHz SiO_2 quartz crystals from Q-Sense. Before each measurement SiO_2-coated crystals are cleaned in a 2% (w/v) sodium dodecyl sulfate (SDS) solution for 15 min, rinsed extensively with distilled water, dried under a stream of nitrogen gas, and exposed to a UV/ozone cleaner (Bioforce Nanoscience, model UV.TC:220) for at least 30 min. The UV light cleans the SiO_2 by eliminating organic contaminants and oxidizing the silicon surface, rendering it hydrophilic. After cleaning, crystals are immediately mounted in the

QCM chamber. All buffer solutions used for QCM measurements are degassed for 1 h using a 2510 Branson Sonicator with degas function (Branson Ultrasonic) immediately before use. The QCM measurements are performed using a QCM-Z500 resonator from KSV (Finland) with dissipation monitoring, equipped with a flow module. The sample is continuously delivered to the measurement chamber by a syringe pump (KD Scientific, model KDS120) at a flow rate of 50 μL/min. All measurements are performed at 23 ± 0.5°C, the temperature being controlled internally by a Peltier heat pump and externally by a refrigerated thermoblock (Nahita model 603/20). After obtaining a stable baseline, a temperature-equilibrated 0.1 mg/mL proteoliposome solution is injected into the QCM chamber. The excess of nonadsorbed proteoliposomes was removed from the chamber by rinsing with buffer (Gutiérrez-Sanz et al., 2016).

Acknowledgments

This work was financially supported by Fundação para a Ciência e Tecnologia (Portugal) through a fellowship SFRH/BD/100314/2014 (to S.Z.), grant PTDC/BBB-BEP/2885/2014 (to P.M.M. and I.A.C.P.), and R&D units UID/Multi/04551/2013 (GreenIT) and LISBOA-01-0145-FEDER-007660 (MostMicro) cofunded by FCT/MCTES and FEDER funds through COMPETE2020/POCI. Funding from the European Unions Horizon 2020 research and innovation program under grant agreement No 810856 and from MINECO/FEDER (projects CTQ2015-71290-R and FIS2015-70339-C2-2-R) is also acknowledged.

References

Abrahams, J. P., & Leslie, A. G. W. (1996). Methods used in the structure determination of bovine mitochondrial F1 ATPase. *Acta Crystallographica Section D: Biological Crystallography*, *52*(1), 30–42. https://doi.org/10.1107/S0907444995008754.

Adams, P. D., Afonine, P. V., Bunkóczi, G., Chen, V. B., Davis, I. W., Echols, N., et al. (2010). PHENIX: A comprehensive Python-based system for macromolecular structure solution. *Acta Crystallographica Section D: Biological Crystallography*, *66*(2), 213–221. https://doi.org/10.1107/S0907444909052925.

Baltazar, C. S. A., Marques, M. C., Soares, C. M., De Lacey, A. M., Pereira, I. A. C., & Matias, P. M. (2011). Nickel-iron-selenium hydrogenases—An overview. *European Journal of Inorganic Chemistry*, *2011*(7), 948–962. https://doi.org/10.1002/ejic.201001127.

Brandis, A., & Thauer, R. K. (1981). Growth of Desulfovibrio species on hydrogen and sulphate as sole energy source. *Microbiology*, *126*(1), 249–252. https://doi.org/10.1099/00221287-126-1-249.

Bricogne, G., Vonrhein, C., Flensburg, C., Schiltz, M., & Paciorek, W. (2003). Generation, representation and flow of phase information in structure determination: Recent developments in and around SHARP 2.0. *Acta Crystallographica Section D: Biological Crystallography*, *59*, 2023–2030. https://doi.org/10.1107/S0907444903017694.

Brünger, A. T. (1992). Free R value: A novel statistical quantity for assessing the accuracy of crystal-structures. *Nature*, *355*(6359), 472–475. https://doi.org/10.1038/355242a0.

Caffrey, S. M., Park, H.-S., Voordouw, J. K., He, Z., Zhou, J., & Voordouw, G. (2007). Function of periplasmic hydrogenases in the sulfate-reducing bacterium Desulfovibrio vulgaris Hildenborough. *Journal of Bacteriology*, *189*(17), 6159–6167. https://doi.org/10.1128/JB.00747-07.

Caputo, C. A., Gross, M. A., Lau, V. W., Cavazza, C., Lotsch, B. V., & Reisner, E. (2014). Photocatalytic hydrogen production using polymeric carbon nitride with a hydrogenase and a bioinspired synthetic Ni Catalyst. *Angewandte Chemie International Edition*, *126*(43), 11538–11542. https://doi.org/10.1002/anie.201406811.

Caputo, C. A., Wang, L., Beranek, R., & Reisner, E. (2015). Carbon nitride-TiO_2 hybrid modified with hydrogenase for visible light driven hydrogen production. *Chemical Science*, *6*(10), 5690–5694. https://doi.org/10.1039/C5SC02017D.

Cowtan, K. (1994). "Dm": An automated procedure for phase improvement by density modification. *Joint CCP4 and ESF-EACBM Newsletter on Protein Crystallography*, *31*, 34–38.

De Lacey, A. L., Fernández, V. M., Rousset, M., & Cammack, R. (2007). Activation and inactivation of hydrogenase function and the catalytic cycle: Spectroelectrochemical studies. *Chemical Reviews*, *107*(10), 4304–4330. https://doi.org/10.1021/cr0501947.

De Lacey, A. L., Gutiérrez-Sánchez, C., Fernández, V. M., Pacheco, I., & Pereira, I. A. C. (2008). FTIR spectroelectrochemical characterization of the Ni-Fe-Se hydrogenase from Desulfovibrio vulgaris Hildenborough. *Journal of Biological Inorganic Chemistry*, *13*(8), 1315–1320. https://doi.org/10.1007/s00775-008-0412-5.

Dong, A., Nam, H., Zhang, J., Andrei, V., Heidary, N., Wagner, A., et al. (2018). Solar water splitting with a hydrogenase integrated in photoelectrochemical tandem cells. *Angewandte Chemie International Edition*, *57*, 10595–10599. https://doi.org/10.1002/anie.201805027.

Emsley, P., Lohkamp, B., Scott, W. G., & Cowtan, K. (2010). Features and development of Coot. *Acta Crystallographica Section D: Biological Crystallography*, *66*(4), 486–501. https://doi.org/10.1107/S0907444910007493.

Evans, G., & Pettifer, R. F. (2001). CHOOCH: A program for deriving anomalous-scattering factors from X-ray fluorescence spectra. *Journal of Applied Crystallography*, *34*, 82–86.

Garcin, E., Vernede, X., Hatchikian, E. C., Volbeda, A., Frey, M., & Fontecilla-Camps, J. C. (1999). The crystal structure of a reduced [NiFeSe] hydrogenase provides an image of the activated catalytic center. *Structure (London, England: 1993)*, 7(5), 557–566. Available at: http://www.ncbi.nlm.nih.gov/pubmed/10378275.

Gutiérrez-Sánchez, C., Olea, D., Marques, M. C., Fernández, V. M., Pereira, I. A. C., Vélez, M., et al. (2011). Oriented immobilization of a membrane-bound hydrogenase onto an electrode for direct electron transfer. *Langmuir: The ACS Journal of Surfaces and Colloids*, *27*(10), 6449–6457. https://doi.org/10.1021/la200141t.

Gutiérrez-Sanz, O., Marques, M. C., Baltazar, C. S. A., Fernández, V. M., Soares, C. M., Pereira, I. A. C., et al. (2013). Influence of the protein structure surrounding the active site on the catalytic activity of [NiFeSe] hydrogenases. *Journal of Biological Inorganic Chemistry*, *18*(4), 419–427. https://doi.org/10.1007/s00775-013-0986-4.

Gutiérrez-Sanz, O., Marques, M. C., Pereira, I. A. C., De Lacey, A. L., Lubitz, W., & Rüdiger, O. (2013). Orientation and function of a membrane-bound enzyme monitored by electrochemical surface-enhanced infrared absorption spectroscopy. *Journal of Physical Chemistry Letters*, *4*(17), 2794–2798. https://doi.org/10.1021/jz4013678.

Gutiérrez-Sanz, O., Natale, P., Márquez, I., Marques, M. C., Zacarias, S., Pita, M., et al. (2016). H_2-fueled ATP synthesis on an electrode: Mimicking cellular respiration. *Angewandte Chemie International Edition*, *55*(21), 6216–6220. https://doi.org/10.1002/anie.201600752.

Gutiérrez-Sanz, O., Tapia, C., Marques, M. C., Zacarias, S., Vélez, M., Pereira, I. A. C., et al. (2015). Induction of a proton gradient across a gold-supported biomimetic membrane by electroenzymatic H_2 oxidation. *Angewandte Chemie International Edition*, *54*, 2684–2687. https://doi.org/10.1002/anie.201411182.

Hedderich, R. (2004). Energy-converting [NiFe] hydrogenases from archaea and extremophiles: Ancestors of complex I. *Journal of Bioenergetics and Biomembranes*, *36*(1), 65–75. https://doi.org/10.1023/B:JOBB.0000019599.43969.33.

Kabsch, W. (1993). Automatic processing of rotation diffraction data from crystals of initially unknown symmetry land cell constants. *Journal of Applied Crystallography*, *26*(Pt. 6), 795–800. https://doi.org/10.1107/S0021889893005588.

Keller, K. L., Bender, K. S., & Wall, J. D. (2009). Development of a markerless genetic exchange system for Desulfovibrio vulgaris Hildenborough and its use in generating a strain with increased transformation efficiency. *Applied and Environmental Microbiology*, *75*(24), 7682–7691. https://doi.org/10.1128/AEM.01839-09.

Keller, K. L., Wall, J. D., & Chhabra, S. (2011). Methods for engineering sulfate reducing bacteria of the genus *Desulfovibrio*. In *Methods in enzymology*. (1st ed.). Elsevier Inc. https://doi.org/10.1016/B978-0-12-385075-1.00022-6

Lee, C. Y., Park, H. S., Fontecilla-Camps, J. C., & Reisner, E. (2016). Photoelectrochemical H_2 evolution with a hydrogenase immobilized on a TiO_2-protected silicon electrode. *Angewandte Chemie International Edition*, *55*(20), 5971–5974. https://doi.org/10.1002/anie.201511822.

Li, M. Z., & Elledge, S. J. (2007). Harnessing homologous recombination in vitro to generate recombinant DNA via SLIC. *Nature Methods*, *4*(3), 251–256. https://doi.org/10.1038/NMETH1010.

Lucena, R., Aguilera, I., Palacios, P., Wahnón, P., & Conesa, J. C. (2008). Synthesis and spectral properties of nanocrystalline V-substituted In_2S_3, a novel material for more efficient use of solar radiation. *Chemistry of Materials*, *20*(16), 5125–5127. https://doi.org/10.1021/cm801128b.

Maroney, M. J., & Hondal, R. J. (2018). Selenium versus sulfur: Reversibility of chemical reactions and resistance to permanent oxidation in proteins and nucleic acids. *Free Radical Biology and Medicine*, *127*, 228–237. https://doi.org/10.1016/j.freeradbiomed.2018.03.035.

Marques, M. C., Coelho, R., De Lacey, A. L., Pereira, I. A. C., & Matias, P. M. (2010). The three-dimensional structure of [NiFeSe] hydrogenase from Desulfovibrio vulgaris Hildenborough: A hydrogenase without a bridging ligand in the active site in its oxidised, "as-isolated" state. *Journal of Molecular Biology*, *396*(4), 893–907. https://doi.org/10.1016/j.jmb.2009.12.013.

Marques, M. C., Coelho, R., Pereira, I. A. C., & Matias, P. M. (2009). Purification, crystallization and preliminary crystallographic analysis of the [NiFeSe] hydrogenase from Desulfovibrio vulgaris Hildenborough. *Acta Crystallographica. Section F, Structural Biology and Crystallization Communications*, *65*(Pt. 9), 920–922. https://doi.org/10.1107/S1744309109031261.

Marques, M. C., Coelho, R., Pereira, I. A. C., & Matias, P. M. (2013). Redox state-dependent changes in the crystal structure of [NiFeSe] hydrogenase from Desulfovibrio vulgaris Hildenborough. *International Journal of Hydrogen Energy*, *38*(21), 8664–8682. https://doi.org/10.1016/j.ijhydene.2013.04.132.

Marques, M. C., Tapia, C., Gutiérrez-Sanz, O., Ramos, A. R., Keller, K. L., Wall, J. D., et al. (2017). The direct role of selenocysteine in [NiFeSe] hydrogenase maturation and catalysis. *Nature Chemical Biology*, *13*(5), 544–550. https://doi.org/10.1038/nchembio.2335.

Matias, P. M., Soares, C. M., Saraiva, L. M., Coelho, R., Morais, J., Le Gall, J., et al. (2001). [NiFe] hydrogenase from Desulfovibrio desulfuricans ATCC 27774: Gene sequencing, three-dimensional structure determination and refinement at 1.8 Å and modelling studies

of its interaction with the tetrahaem cytochrome c3. *Journal of Biological Inorganic Chemistry*, *6*(1), 63–81. https://doi.org/10.1007/s007750000167.

McCoy, A. J. (2006). Solving structures of protein complexes by molecular replacement with Phaser. *Acta Crystallographica Section D: Biological Crystallography*, *63*(1), 32–41. https://doi.org/10.1107/S0907444906045975.

Mersch, D., Lee, C., Zhang, J. Z., Brinkert, K., Fontecilla-camps, J. C., Rutherford, A. W., et al. (2015). Wiring of photosystem II to hydrogenase for photoelectrochemical water splitting. *Journal of the American Chemical Society*, *137*, 8541–8549. https://doi.org/10.1021/jacs.5b03737.

Moss, D., Nabedryk, E., Breton, J., & Mantele, W. (1990). Redox-linked conformational changes in proteins detected by a combination of infrared spectroscopy and protein electrochemistry: Evaluation of the technique with cytochrome c. *European Journal of Biochemistry*, *187*(3), 565–572. https://doi.org/10.1111/j.1432-1033.1990.tb15338.x.

Murshudov, G. N., Skubák, P., Lebedev, A. A., Pannu, N. S., Steiner, R. A., Nicholls, R. A., et al. (2011). REFMAC5 for the refinement of macromolecular crystal structures. *Acta Crystallographica Section D: Biological Crystallography*, *67*(4), 355–367. https://doi.org/10.1107/S0907444911001314.

Muth, E., Morschel, E., & Klein, A. (1987). Purification and characterization of an 8-hydroxy-5-deazaflavin-reducing hydrogenase from the archaebacterium Methanococcus voltae. *European Journal of Biochemistry*, *169*(3), 571–577. https://doi.org/10.1111/j.1432-1033.1987.tb13647.x.

Nonaka, K., Nguyen, N. T., Yoon, K.-S., & Ogo, S. (2013). Novel H_2-oxidizing [NiFeSe] hydrogenase from Desulfovibrio vulgaris Miyazaki F. *Journal of Bioscience and Bioengineering*, *115*(4), 366–371. https://doi.org/10.1016/j.jbiosc.2012.10.011.

Painter, J., & Merritt, E. A. (2006). Optimal description of a protein structure in terms of multiple groups undergoing TLS motion. *Acta Crystallographica Section D: Biological Crystallography*, *62*(4), 439–450. https://doi.org/10.1107/S0907444906005270.

Pape, T., & Schneider, T. R. (2004). HKL2MAP: A graphical user interface for macromolecular phasing with SHELX programs. *Journal of Applied Crystallography*, *37*(5), 843–844. https://doi.org/10.1107/S0021889804018047.

Papp, L. V., Lu, J., Holmgren, A., & Khanna, K. K. (2007). From selenium to selenoproteins: Synthesis, identity, and their role in human health. *Antioxidants & Redox Signaling*, *9*(7), 775–806. https://doi.org/10.1089/ars.2007.1528.

Parkin, A., Goldet, G., Cavazza, C., Fontecilla-Camps, J. C., & Armstrong, F. A. (2008). The difference a Se makes? Oxygen-tolerant hydrogen production by the [NiFeSe]-hydrogenase from Desulfomicrobium baculatum. *Journal of the American Chemical Society*, *130*(40), 13410–13416. https://doi.org/10.1021/ja803657d.

Pereira, I. A. C., Ramos, A. R., Grein, F., Marques, M., da Silva, S. M., & Venceslau, S. S. (2011). A comparative genomic analysis of energy metabolism in sulfate reducing bacteria and archaea. *Frontiers in Microbiology*, *2*, 69. https://doi.org/10.3389/fmicb.2011.00069.

Pereira, I. A. C., Romão, C. V., Xavier, A. V., Le Gall, J., & Teixeira, M. (1998). Electron transfer between hydrogenases and mono- and multiheme cytochromes in Desulfovibrio ssp. *Journal of Biological Inorganic Chemistry*, 494–498.

Perrakis, A., Morris, R., & Lamzin, V. S. (1999). Automated protein model building combined with iterative structure refinement. *Nature Structural Biology*, *6*(5), 458–463. https://doi.org/10.1038/8263.

Postgate, J. R. (1984). *Sulphate-reducing bacteria*. London, UK: Cambridge University Press. https://doi.org/10.1017/CBO9780511541490.

Potterton, E., Briggs, P., Turkenburg, M., & Dodson, E. (2003). A graphical user interface to the CCP4 program suite. *Acta Crystallographica, Section D: Biological Crystallography*, *59*(7), 1131–1137. https://doi.org/10.1107/S0907444903008126.

Reich, H. J., & Hondal, R. J. (2016). Why nature chose selenium. *ACS Chemical Biology*, *11*(4), 821–841. https://doi.org/10.1021/acschembio.6b00031.

Reisner, E., Fontecilla-camps, J. C., & Armstrong, F. A. (2009). Catalytic electrochemistry of a [NiFeSe]-hydrogenase on TiO_2 and demonstration of its suitability for visible-light driven H_2 production. *Chemical Communications*, (5), 550–552. https://doi.org/10.1039/b817371k.

Reisner, E., Powell, D. J., Cavazza, C., Fontecilla-Camps, J. C., & Armstrong, F. A. (2009). Visible light-driven H(2) production by hydrogenases attached to dye-sensitized TiO(2) nanoparticles. *Journal of the American Chemical Society*, *131*(51), 18457–18466. https://doi.org/10.1021/ja907923r.

Rodrigue, A., Chanal, A., Beck, K., Müller, M., Wu, L., & Mu, M. (1999). Co-translocation of a periplasmic enzyme complex by a hitchhiker mechanism through the bacterial tat pathway. *The Journal of Biological Chemistry*, *274*(19), 13223–13228. https://doi.org/10.1074/jbc.274.19.13223.

Rüdiger, O., Gutiérrez-Sánchez, C., Olea, D., Pereira, I. A. C., Vélez, M., Fernández, V. M., et al. (2010). Enzymatic anodes for hydrogen fuel cells based on covalent attachment of Ni-Fe hydrogenases and direct electron transfer to SAM-modified gold electrodes. *Electroanalysis*, *22*(7–8), 776–783. https://doi.org/10.1002/elan.200880002.

Ruff, A., Szczesny, J., Zacarias, S., Pereira, I. A. C., Plumeré, N., & Schuhmann, W. (2017). Protection and reactivation of the [NiFeSe] hydrogenase from Desulfovibrio vulgaris Hildenborough under oxidative conditions. *ACS Energy Letters*, *2*(5). https://doi.org/10.1021/acsenergylett.7b00167.

Ruff, A., Szczesny, J., Marković, N., Conzuelo, F., Zacarias, S., Pereira, I. A. C., et al. (2018). A fully protected hydrogenase/polymer-based bioanode for high-performance hydrogen/glucose biofuel cells. *Nature Communications*, *9*(1), 3675. https://doi.org/10.1038/s41467-018-06106-3.

Sakai, T., Mersch, D., & Reisner, E. (2013). Photocatalytic hydrogen evolution with a hydrogenase in a mediator-free system under high levels of oxygen. *Angewandte Chemie (International ed. in English)*, *52*(47), 12313–12316. https://doi.org/10.1002/anie.201306214.

Schneider, T. R., & Sheldrick, G. M. (2002). Substructure solution with SHELXD. *Acta Crystallographica Section D: Biological Crystallography*, *58*(10), 1772–1779. https://doi.org/10.1107/S0907444902011678.

Sheldrick, G. M. (2002). Macromolecular phasing with SHELXE. *Zeitschrift für Kristallographie*, *217*(12), 644–650.

Sheldrick, G. M. (2010). Experimental phasing with SHELXC/D/E: Combining chain tracing with density modification. *Acta Crystallographica Section D: Biological Crystallography*, *66*(4), 479–485. https://doi.org/10.1107/S0907444909038360.

Tapia, C., Zacarias, S., Pereira, I. A. C., Conesa, J. C., Pita, M., & De Lacey, A. L. (2016). In situ determination of photobioproduction of H_2 by In_2S_3-[NiFeSe] hydrogenase from Desulfovibrio vulgaris Hildenborough using only visible light. *ACS Catalysis*, *6*(9), 5691–5698. https://doi.org/10.1021/acscatal.6b01512.

Teixeira, M., Fauque, G., Moura, I., Lespinat, P. A., Berlier, Y., Prickril, B., Jr., et al. (1987). Nickel-[iron-sulfur]-selenium-containing hydrogenases from Desulfovibrio baculatus (DSM 1743). *European Journal of Biochemistry*, *58*, 47–58. https://doi.org/10.1111/j.1432-1033.1987.tb13302.

Teixeira, M., Moura, I., Fauque, G., Czechowski, M., Berlier, Y., Lespinat, P. A., et al. (1986). Redox properties and activity studies on a nickel-containing hydrogenase isolated from a halophilic sulfate reducer Desulfovibrio salexigens. *Biochimie*, *68*, 75–84. https://doi.org/10.1016/S0300-9084(86)81071-9.

Valente, F. M. A., Almeida, C., Pacheco, I., Saraiva, M., & Pereira, I. A. C. (2006). Selenium is involved in regulation of periplasmic hydrogenase gene expression in Desulfovibrio vulgaris Hildenborough. *Journal of Bacteriology*, *188*(9), 3228–3235. https://doi.org/10.1128/JB.188.9.3228.

Valente, F. M. A., Oliveira, A. S. F., Gnadt, N., Pacheco, I., Coelho, A. V., Xavier, A. V., et al. (2005). Hydrogenases in Desulfovibrio vulgaris Hildenborough: Structural and physiologic characterisation of the membrane-bound [NiFeSe] hydrogenase. *Journal of Biological Inorganic Chemistry*, *10*(6), 667–682. https://doi.org/10.1007/s00775-005-0022-4.

Valente, F. M. A., Pereira, P. M., Venceslau, S. S., Regalla, M., Coelho, A. V., & Pereira, I. A. C. (2007). The [NiFeSe] hydrogenase from Desulfovibrio vulgaris Hildenborough is a bacterial lipoprotein lacking a typical lipoprotein signal peptide. *FEBS Letters*, *581*(18), 3341–3344. https://doi.org/10.1016/j.febslet.2007.06.020.

Vignais, P. M. (2005). H/D exchange reactions and mechanistic aspects of the hydrogenases. *Coordination Chemistry Reviews*, *249*(15–16), 1677–1690. https://doi.org/10.1016/j.ccr.2005.01.026.

Vincent, K. A., Parkin, A., & Armstrong, F. A. (2007). Investigating and exploiting the electrocatalytic properties of hydrogenases. *Chemical Reviews*, *107*(10), 4366–4413. https://doi.org/10.1021/cr050191u.

Winn, M. D., Isupov, M. N., & Murshudov, G. N. (2001). Use of TLS parameters to model anisotropic displacements in macromolecular refinement research papers use of TLS parameters to model anisotropic displacements in macromolecular refinement. *Acta Crystallographica, Section D: Biological Crystallography*, *57*, 122–133.

Yamazaki, S. (1982). A selenium-containing hydrogenase from Methanococcus vannielii. Identification of the selenium moiety as a selenocysteine residue. *The Journal of Biological Chemistry*, *257*, 7926–7929.

Zane, G. M., Yen, H. B., & Wall, J. D. (2010). Effect of the deletion of qmoABC and the promoter-distal gene encoding a hypothetical protein on sulfate reduction in Desulfovibrio vulgaris Hildenborough. *Applied and Environmental Microbiology*, *76*(16), 5500–5509. https://doi.org/10.1128/AEM.00691-10.